Journal of Solid State Chemistry 183 (2010) 2309–2316

Contents lists available at ScienceDirect

Journal of Solid State Chemistry

journal homepage: www.elsevier.com/locate/jssc

Nano/micro-scaled La(1,3,5-BTC)$(H_2O)_6$ coordination polymer: Facile morphology-controlled fabrication and color-tunable photoluminescence properties by co-doping Eu^{3+},Tb^{3+}

Kai Liu [a,b], Yuhua Zheng [a,b], Guang Jia [a,b], Mei Yang [a,b], Yanhua Song [a,b], Ning Guo [a,b], Hongpeng You [a,b,*]

[a] State Key Laboratory of Rare Earth Resource Utilization, Changchun Institute of Applied Chemistry, Chinese Academy of Sciences, Changchun 130022, PR China
[b] Graduate School of the Chinese Academy of Sciences, Beijing 100049, PR China

ARTICLE INFO

Article history:
Received 6 May 2010
Received in revised form
20 July 2010
Accepted 25 July 2010
Available online 3 August 2010

Keywords:
Self-assembly
Luminescence
Hierarchical architecture
Coordination polymer
Crystal growth

ABSTRACT

Nano/micro-sized coordination polymer La(1,3,5-BTC)$(H_2O)_6$ with controllable morphologies have been successfully prepared on a large scale via a simple solution phase method at room temperature. By rationally adjusting the synthetic parameters such as concentration, molar ratio of reactants, surfactant, and solvent, the La(1,3,5-BTC)$(H_2O)_6$ with 3D flowerlike, wheatearlike, spherical, sheaflike, taillike, bundlelike hierarchical architectures, and 1D nanorods can be selectively prepared. More interestingly, the photoluminescence color of codoped Eu^{3+} and Tb^{3+} lanthanum 1,3,5-benzenetricarboxylate phosphors can be easily tuned from red, orange, yellow, green-yellow to green by changing co-doping concentration of activator ions, making the material has potential applications in building miniopto-electronic devices, biomedicine, and color display fields.

© 2010 Elsevier Inc. All rights reserved.

1. Introduction

Coordination polymers or metal–organic frameworks, in which metal ions or metal clusters are connected by molecular building blocks consisting of organic molecules or organometallic complexes, have received a great deal of attention due to their useful applications in gas storage, catalysis, optics, recognition, and separation [1–4]. Thus, much attention has been devoted to the study of macro-scaled crystalline samples in metal-organic fields. Recently, with the development of nanoscience and nanotechnology, several micro- and nanometer-sized metal-organic complexes have been synthesized. For example, Mirkin's group demonstrated the formation of chemically tailorable spherical coordination polymer particles by simply adding an initiation solvent to a precursor solution containing metal ions and metalloligands [5]. Masel's group prepared micro-sized cubic coordination polymer particles via a microwave-assisted solvothermal synthetic method [6]. Lin et al. reported the preparation of nano-scaled metal-organic frameworks based on Ln^{3+} and BDC (BHC) through microemulsion and hydrothermal methodology [7]. Oh et al. also described a solvothermal approach for the synthesis of coordination polymer to study morphological transformation [8]. Li's group successfully synthesized composite nanofibrous membranes as optical oxygen sensors based on low-cost Cu(I) complexes by electrospinning [9]. These works suggest that the suitable design of reaction routes and selection of the metal ions and organic ligands could open a new field for preparing nano- or micro-scaled metal–organic materials for potential uses in minioptoelectronics, imaging, biosensing, drug delivery, and so on [10,11].

Benzenetricarboxylate are widely used in the construction of high-dimensional lanthanide coordination complexes because these anions are able to act as bridging ligands in various ligating modes [12–15]. By choosing 1,3,5-benzenetricarboxylate (1,3,5-BTC) as bridging ligands and lanthanide ions as metal connectors, we recently have successfully prepared a series of coordination polymer Ln(1,3,5-BTC)$(H_2O)_6$ (Ln=Eu^{3+}, La^{3+}, and Ce^{3+}) 3D superstructures and 1D nanorods and metal–organic framework Tb(1,3,5-BTC)$(H_2O)\cdot 3H_2O$ 1D nanobelts via direct precipitation in solution phase [16–18]. For example, well-dispersed 3D straw-sheaflike, broccolilike, urchinlike, and fanlike architectures of La(1,3,5-BTC)$(H_2O)_6$ have been prepared by vigorous stirring, static, and ultrasonic treatment in solution phase at room temperature, respectively [18]. And white light emission of the La(1,3,5-BTC)$(H_2O)_6$ superstructures were realized by co-doping Eu^{3+} and Tb^{3+} when the UV excitation wavelength was controlled from 325 to 329 nm. As a continuation and extension of this work, here we mainly focused on the effects of the reaction parameters such as concentration, molar ratio of reactants, surfactant, and

* Corresponding author at: State Key Laboratory of Rare Earth Resource Utilization, Changchun Institute of Applied Chemistry, Chinese Academy of Sciences, Changchun 130022, PR China. Fax: +86 431 85698041.
E-mail address: hpyou@ciac.jl.cn (H. You).

0022-4596/$ - see front matter © 2010 Elsevier Inc. All rights reserved.
doi:10.1016/j.jssc.2010.07.040

solvent on morphologies of the La(1,3,5-BTC)$(H_2O)_6$ crystals (under vigorous stirring conditions); and flowerlike, wheatearlike, spherical, sheaflike, taillike, bundlelike architectures, and nanorods were selectively obtained. In addition, tunable photoluminescence from red, orange, yellow, green-yellow to green of the La(1,3,5-BTC)$(H_2O)_6$:Eu^{3+},Tb^{3+} nano/microstructures were achieved successfully by tuning the codopant concentration and excitation wavelength.

2. Experimental

2.1. Preparation

Ln$(NO_3)_3$ (*Ln*=La, Eu, Tb) aqueous solution was obtained by dissolving La_2O_3, Eu_2O_3, and Tb_4O_7 in dilute HNO_3 solution under heating with agitation, respectively. In a typical synthesis of La(1,3,5-BTC)$(H_2O)_6$, 2 mL of 0.5 M La$(NO_3)_3$ aqueous solution was added into 1,3,5-benzenetricarboxylic acid (1,3,5-H_3BTC, 1 mmol) water–ethanol solution (40 mL, v/v=1:1) under vigorous stirring at room temperature and a large amount of white precipitate occurred immediately. After reaction for 15 min, the precipitate was collected by centrifugation, washed several times with ethanol and water, and dried in air for characterization. La(1,3,5-BTC)$(H_2O)_6$ with different forms of splitting such as flowerlike, wheatearlike, spherical, sheaflike, taillike, bundlelike architectures, and nanorods were carried out by adjusting concentrations of 1,3,5-BTC and La$(NO_3)_3$ (0.05, 3, 4 mmol each), molar ratio of 1,3,5-H_3BTC to La (1:4 mmol), the amount of polyvinylpyrrolidone (PVP K30, M=58,000, 1.0 g), water–ethanol ratio (40 mL, v/v=3:1), and ethanol as the solvent (40 mL) with other fixed reaction parameters.

A similar process was employed to prepare Eu^{3+} and Tb^{3+}-doped La(1,3,5-BTC)$(H_2O)_6$ nano/microstructures except for adding a certain amount of Eu$(NO_3)_3$ (co-doping concentration: 1 mol%) and Tb$(NO_3)_3$ (co-doping concentration: 1–9 mol%) into La$(NO_3)_3$ solution at the initial stage while other reaction parameters kept unchanged.

2.2. Characterization

Powder X-ray diffraction (XRD) patterns were performed on a D8 Focus (Bruker) diffractometer (continuous, 40 kV, 40 mA, increment=0.02°). The morphology and composition of the samples were inspected using a scanning electron microscope (SEM, S-4800, Hitachi) equipped with an energy dispersive X-ray spectrum (EDX, JEOL JXA-840). Photoluminescence excitation and emission spectra were recorded with a Hitachi F-4500 spectrophotometer equipped with a 150 W xenon lamp as the excitation source. All the measurements were performed at room temperature.

3. Results and discussion

3.1. Phase identification of the La(1,3,5-BTC)$(H_2O)_6$

The chemical composition and crystal structure of the samples were determined by X-ray powder diffraction (XRD) measurements. The XRD patterns of the as-synthesized La(1,3,5-BTC)$(H_2O)_6$ with different morphologies show that the products are crystalline in spite of the moderate reaction conditions (Fig. 1). All the diffraction peaks of the products can be well indexed to the known bulk phase [14] and our reported nano/microstructure [18] of La(1,3,5-BTC)$(H_2O)_6$. The crystal structure of the as-obtained samples can thus be of monoclinic, space group *Cc*.

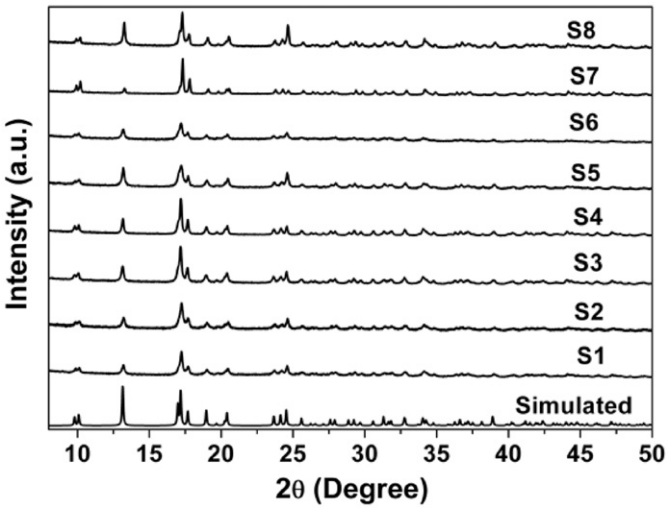

Fig. 1. Simulated XRD pattern using the X-ray structure of La(1,3,5-BTC)$(H_2O)_6$ single crystal and XRD patterns of the La(1,3,5-BTC)$(H_2O)_6$ prepared under different conditions: S1 (1:1 mmol), S2 (0.05:0.05 mmol), S3 (3:3 mmol), S4 (4:4 mmol), S5 (1,3,5-H_3BTC/La=1:4 mmol), S6 (1:1 mmol, 1.0 g PVP), S7 (1:1 mmol, ethanol–water (v/v=1:3), 40 mL), S8 (0.5:0.5 mmol, ethanol, 40 mL).

The interesting feature of the La(1,3,5-BTC)$(H_2O)_6$ is the presence of parallel 1D ribbonlike structure. In addition, no peaks of impurities are detected from the XRD patterns of La(1,3,5-BTC)$(H_2O)_6$:Eu^{3+},Tb^{3+}, indicating that the samples are isostructural with the La(1,3,5-BTC)$(H_2O)_6$ and the Eu^{3+} and Tb^{3+} ions have been effectively incorporated into the La(1,3,5-BTC)$(H_2O)_6$ host lattice (Fig. S1, Supporting Information).

Furthermore, the chemical composition of the La(1,3,5-BTC)$(H_2O)_6$ and La(1,3,5-BTC)$(H_2O)_6$:Eu^{3+},Tb^{3+} nano/microstructures was further investigated with EDX spectra (Fig. S2). The results confirm that the samples are made of La, C, O, and corresponding Eu, Tb except the Si and Pt peaks from measurements.

3.2. Influences of different reaction parameters on the morphologies of La(1,3,5-BTC)$(H_2O)_6$

In a typical synthesis of La(1,3,5-BTC)$(H_2O)_6$, 2 mL of 0.5 M La$(NO_3)_3$ aqueous solution was added into 1,3,5-benzenetricarboxylic acid (1,3,5-H_3BTC, 1 mmol) water–ethanol solution (40 mL, v/v=1:1) under vigorous stirring at room temperature. The La(1,3,5-BTC)$(H_2O)_6$ took place splitting growth [19] and straw-sheaflike architectures with lengths of 4–6 μm were obtained, which are similar to our reported work [18] (Fig. S3). However, when we controlled the synthetic parameters such as concentration, molar ratio of reactants, surfactant, and solvent reasonably, the La(1,3,5-BTC)$(H_2O)_6$ can take on different splitting forms. Thus, 3D flowerlike, wheatearlike, spherical, sheaflike, taillike, bundlelike hierarchical architectures, and 1D nanorods can be selectively prepared. The results of the morphology evolution under different reaction conditions are summarized in Table 1.

3.2.1. Effects of concentration

It is believed that crystal splitting is associated with fast crystal growth, which depends strongly on the oversaturation of the solution [19]. Variation in the concentration of reactants resulted in successive splitting of the La(1,3,5-BTC)$(H_2O)_6$ architectures. Fig. 2 shows the SEM images of morphologies obtained at low concentrations of 1,3,5-H_3BTC and La$(NO_3)_3$ (0.05 mmol each) while keeping other reaction conditions the same. Surprisingly, a

Table 1
Summary of the experimental conditions and the corresponding morphologies of the La(1,3,5-BTC)$(H_2O)_6$ samples.

Sample	Concentration (mmol)	1,3,5-H_3BTC/La^{3+}	PVP (g)	Water/ethanol	Morphology	Length (μm)
S1	1:1	1:1	0	1:1	Straw-sheaf	4–6
S2	0.05:0.05	1:1	0	1:1	Flower	2–3
S3	3:3	1:1	0	1:1	Wheatear	2
S4	4:4	1:1	0	1:1	Nanorod	5–10
S5	1:4	1:4	0	1:1	Sphere	5
S6	1:1	1:1	1.0	1:1	Sheaf	2–3
S7	1:1	1:1	0	3:1	Tail	3
S8	1:1	1:1	0	Pure ethanol	Bundle	2

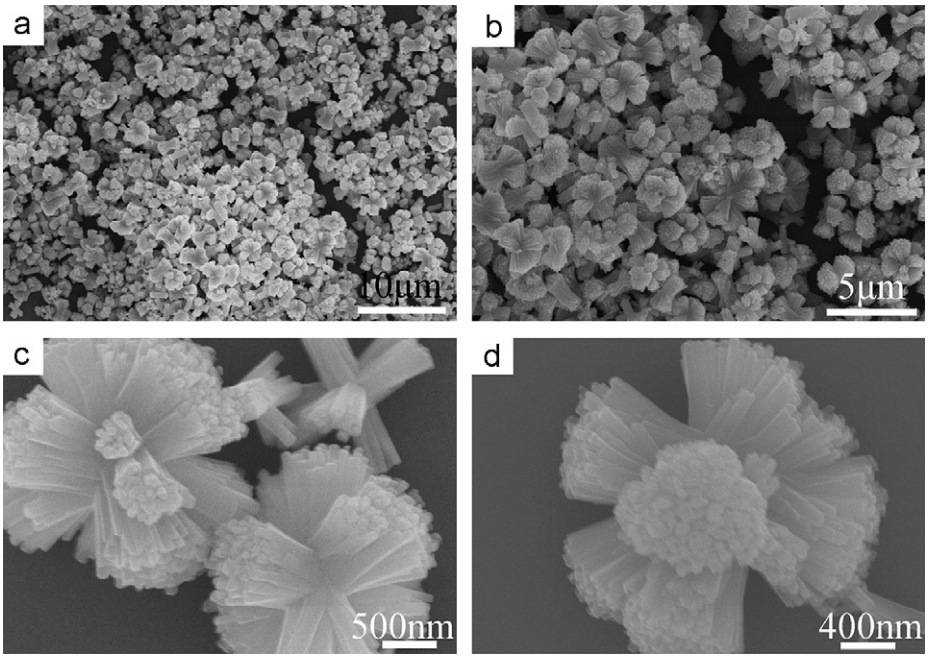

Fig. 2. SEM images (a)–(d) of the La(1,3,5-BTC)$(H_2O)_6$ flowerlike architectures at different magnifications (0.05:0.05 mmol).

large quantity of beautiful microflower architectures consisting of well-aligned nanorods appeared from the low-magnification SEM image (Fig. 2a and b). From the enlarged SEM image shown in Fig. 2c and d, the La(1,3,5-BTC)$(H_2O)_6$ flowers with lengths of 2–3 μm have some petals and a central nucleus. These superstructures are composed of numerous nanorods pointing toward the center of flowerlike structures, exhibiting obvious splitting. As the concentrations of 1,3,5-BTC and $La(NO_3)_3$ was increased to 1 mmol, uniform hierarchical straw-sheaflike architectures made of abundant nanorods with very high density were obtained on a large scale (Fig. S3). When the concentrations reached 3 mmol, more interestingly, a large quantity of wheatearlike structures with simple splitting were obtained, which are composed of several nanorods (Fig. 3a and b). Close observations indicate that that these La(1,3,5-BTC)$(H_2O)_6$ microstructures look like natural wheatears with lengths of about 2 μm. The nanorods have widths of 80–120 nm and thicknesses of 30–50 nm, respectively. As the concentrations of reactants increased to 4 mmol, splitting growth was strongly inhibited and the trend of anisotropic growth is strengthened. Thus, only 1D rodlike nanostructures were obtained on a large scale (Fig. 3c and d). More careful observations of the typical rodlike structure indicate that the compressed nanorods have widths of 100–200 nm, thicknesses of about 50 nm, and lengths in the range of 5–10 μm, respectively. On the basis of the above results, one can see that the splitting degree of La(1,3,5-BTC)$(H_2O)_6$ decreases as the concentrations of the reactants increase from 0.05 to 4 mmol. It is generally suggested that splitting is only possible if the oversaturation exceeds a certain "critical" level, which is specific for each mineral and the given conditions [20]. However, according to the nucleation and growth theory of nanocrystals, when the concentration is higher, more nuclei will form in a shorter time. And a large number of nuclei will then grow slowly, which will prohibit the occurrence of the splitting growth process [19]. Therefore, 3D flowerlike, straw-sheaflike, wheatearlike hierarchical architectures and 1D nanorods can be selectively obtained via tuning reactants concentrations. It is well known that crystal growth stage is a kinetically and thermodynamically controlled process that can form different shapes with some degree of shape tenability through changes in the reaction parameters [21]. In the present system, the concentration of the reactants is undoubtedly vital in the formation of controllable morphologies of La(1,3,5-BTC)$(H_2O)_6$.

3.2.2. *Effects of molar ratio*

In addition to concentration, the molar ratios of the 1,3,5-H_3BTC to $La(NO_3)_3$ in the binary solution also significantly influenced the morphology of the products. At a molar ratio of 1:1, the as-prepared sample is entirely composed of straw-sheaves with obvious splitting, perfect uniformity, and monodispersity (Fig. S3). However, splitting of the microarchitectures can be enhanced with decreasing 1,3,5-H_3BTC/$La(NO_3)_3$ molar

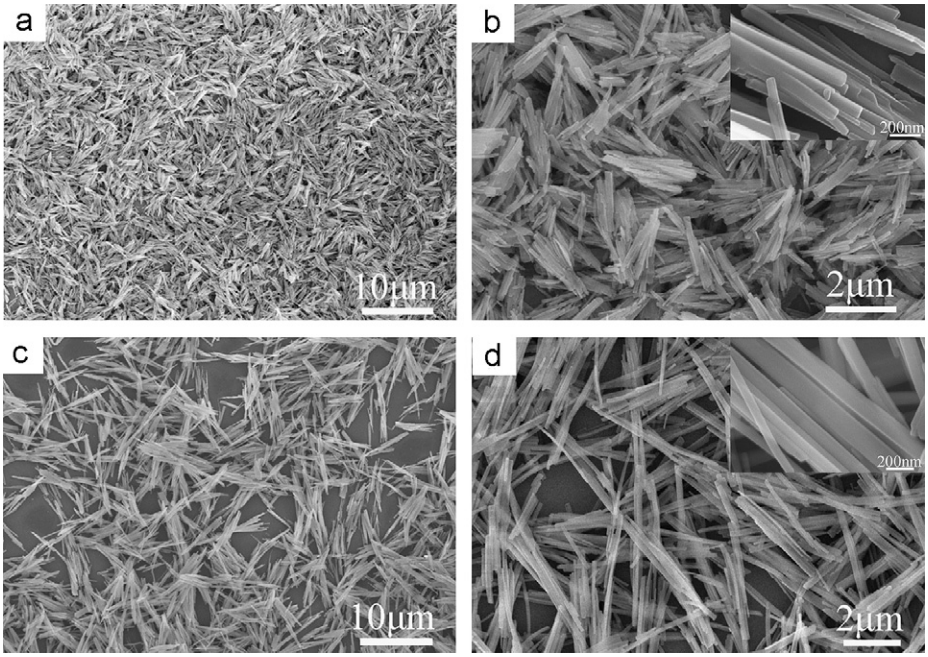

Fig. 3. SEM images of the La(1,3,5-BTC)$(H_2O)_6$ wheatearlike architectures (a, b, 3:3 mmol) and nanorods (c, d, 4:4 mmol) at different magnifications.

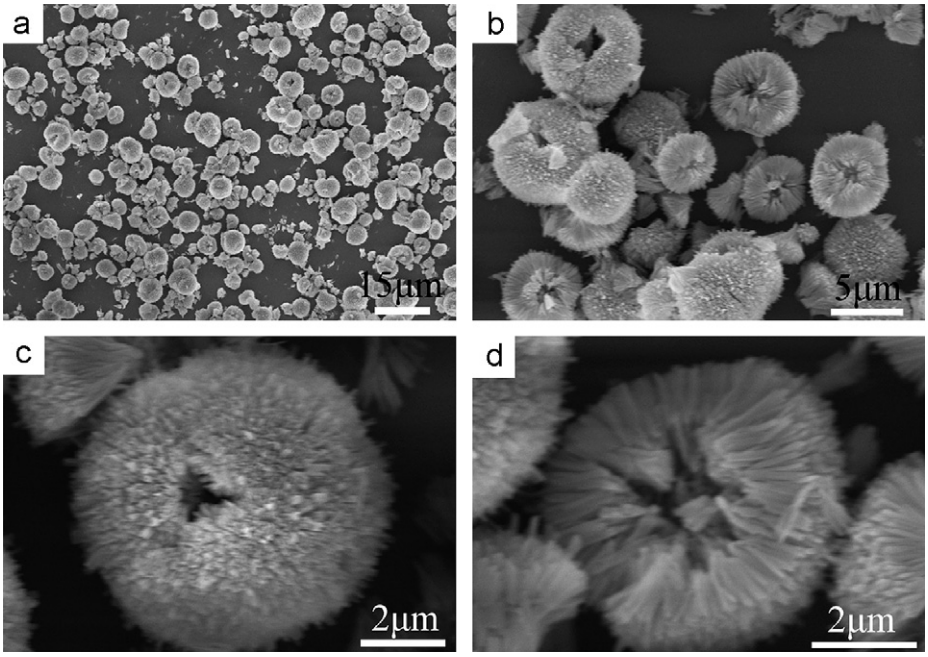

Fig. 4. SEM images of the the La(1,3,5-BTC)$(H_2O)_6$ spherical architectures at different magnifications (1,3,5-H_3BTC/La = 1:4 mmol).

ratio. When the molar ratio decreased to 1:4, spherical architectures with lengths of about 5 μm splitting almost completely from the center part were obtained, which were assembled from well-aligned nanorods with high density (Fig. 4). Interestingly, more careful observations of the typical spherical structure indicate that each sphere has a hole in the middle. The holes are not very regular, which have diameters of 0.5–2 μm. In addition, some detached spherical microstructures with almost complete splitting were also observable. The above observations indicate that the presence of excessive La^{3+} ions could interrupt the crystal growth and crystal splitting, and most importantly result in the morphology evolution easily.

3.2.3. *Effects of surfactants*

Recently, various types of surfactants have been widely used in most solution routes in the synthesis of well structured materials with controlled morphology due to their efficient self-assembly properties [19,22,23]. These surfactants can control the nucleation and crystallization of nanomaterials with special orientation and morphology. Most importantly, the crystal splitting extent could be interrupted in the presence of surfactants. Therefore, we investigated the influence of PVP on the morphological evolution under the typical conditions for straw-sheaflike structures formation (1:1 mmol). When PVP was not used, the product looks like straw-sheaf with two fantails, exhibiting radiating form

(Fig. S3). This morphology character is that a sheaf of rodlike crystals has been bandaged in the middle, with the top and bottom fanning out while the middle remaining thin. However, if some amount of PVP (1.0 g) was added, sheaflike superstructures with no radiating fantails could be obtained on a large scale (Fig. 5a). These sheaves are nearly monodispersed with lengths of 2–3 μm (Fig. 5b). Detailed SEM observations reveal that dual fanlike patterns disappeared and the splitting extent was held back (Fig. 5c and d). The individual nanorods composing the microsheaves are 70–150 nm in width and 10–30 nm in thickness, respectively (Fig. 5e and f). On the basis of the observation, we can reasonably assume that PVP may act as potential crystal face inhibitors and can be preferentially absorbed to some specific planes, which benefits the formation of oriented nucleation and affect the crystal splitting. However, the exact role of PVP in the growth of La(1,3,5-BTC)$(H_2O)_6$ microarchitectures needs further investigation.

3.2.4. *Effects of solvent*

The solvent was an important factor in the morphology evolution of the La(1,3,5-BTC)$(H_2O)_6$. When volume ratio of water/ethanol solution was 1 (40 mL, $v/v=1:1$), we obtained the typical straw-sheaves superstructures with two fantails, which are composed of compressed and straight nanorods (Fig. S3). As the volume ratio of water/ethanol was increased to 3 (40 mL, $v/v=3:1$), taillike architectures with obvious splitting were obtained on a large scale. The first impression is that the La(1,3,5-BTC)$(H_2O)_6$ taillike microstructures with lengths of about 3 μm have opened their tails to a large extent (Fig. 6a and b). Careful observation of the detailed structure reveals that the rodlike crystals have been bandaged in the tip with the bottom fanning out while the tip remaining thin (Fig. 6c and d). The individual nanorods composing the tails are 50–100 nm in width and about 20 nm in thickness, respectively. Furthermore, we also used ethanol instead of water as the single solvent (40 mL) to study the solvent effect on the morphology evolution of the sample. A large quantity of bundlelike superstructures with no radiating fantails could be obtained on a large scale (Fig. 7a). These microbundles are monodispersed with lengths of about 2 μm (Fig. 7b). More detailed studies on the crystal structure reveal that dual fanlike patterns disappeared and the splitting extent was held back (Fig. 7c and d). High magnification SEM image of the sample (inset in Fig. 7d) indicates that the width and thickness of these nanorods are in the range of 60–120 and 20–30 nm, respectively. These observations demonstrate that the change of solution polarity can lead to the different dipole–dipole interactions, which would change the initial speciation, interfere with the nanocrystal growth, kinetically control the progress of splitting, induce the assembly and stacking of La(1,3,5-BTC)$(H_2O)_6$ molecules in different modes, and control the ultimate morphology and size variation of these 3D architectures.

We also investigated the morphology evolution of Ln^{3+}-doped lanthanum 1,3,5-benzenetricarboxylate by controlling concentration, molar ratio of reactants, surfactant, and solvent in solution phase at room temperature. During the synthesis, 3D straw-sheaflike,

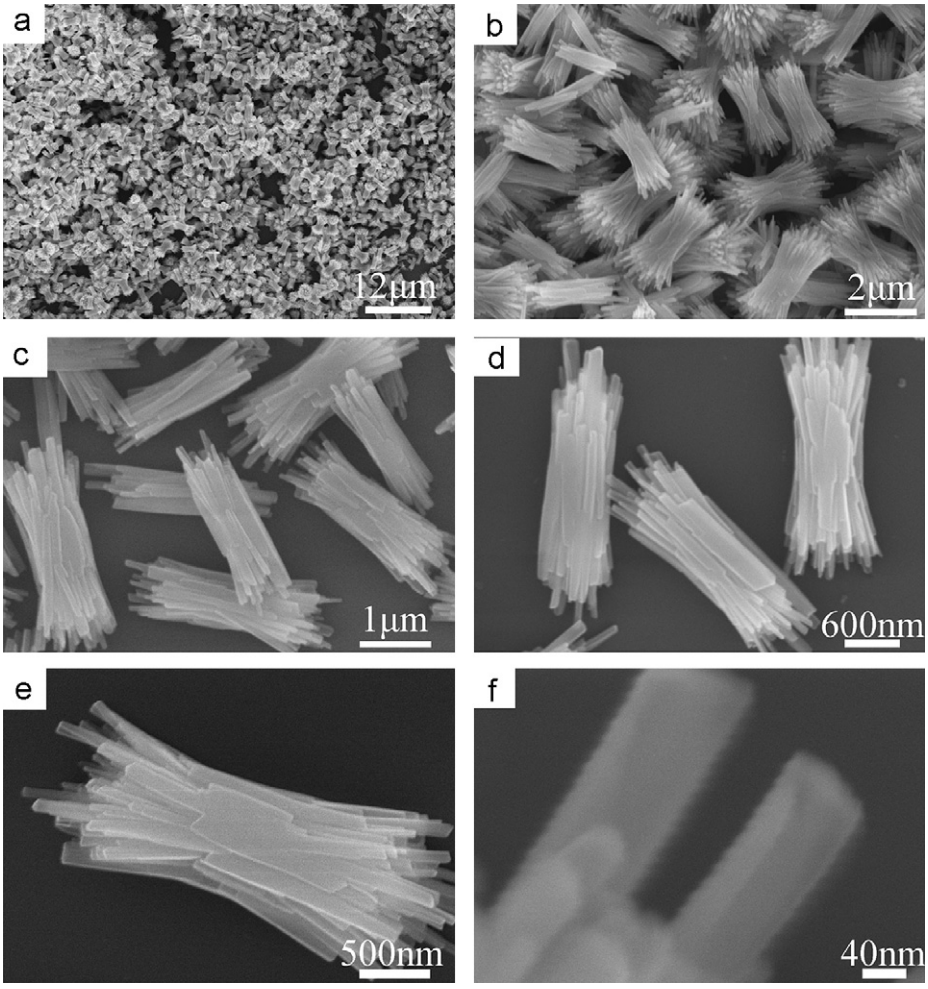

Fig. 5. SEM images of the La(1,3,5-BTC)$(H_2O)_6$ sheaflike architectures at different magnifications (1 g PVP).

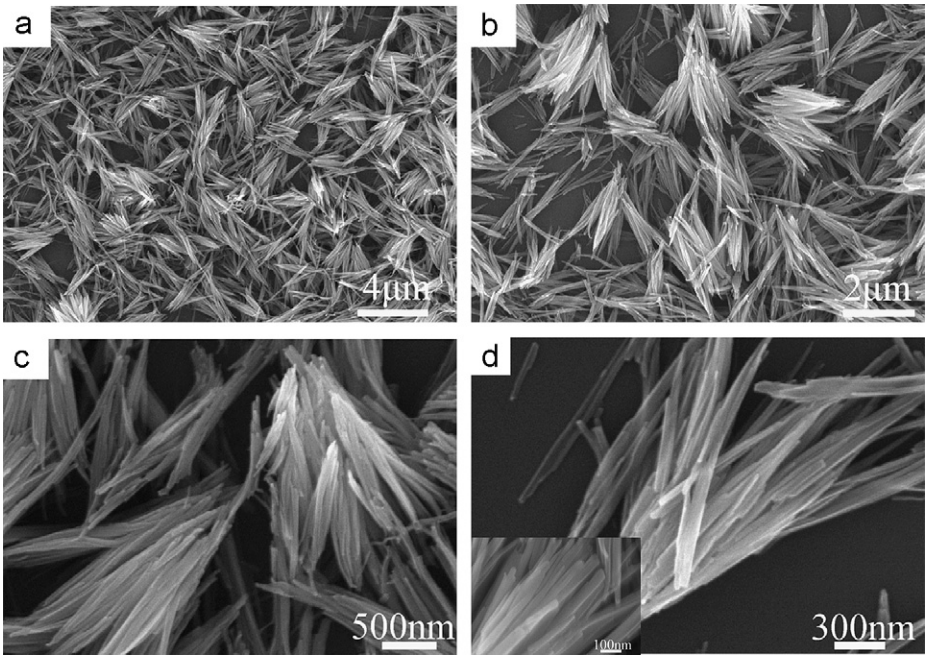

Fig. 6. SEM images of the La(1,3,5-BTC)$(H_2O)_6$ taillike architectures at different magnifications (ethanol–water, $v/v=1:3$, 40 mL).

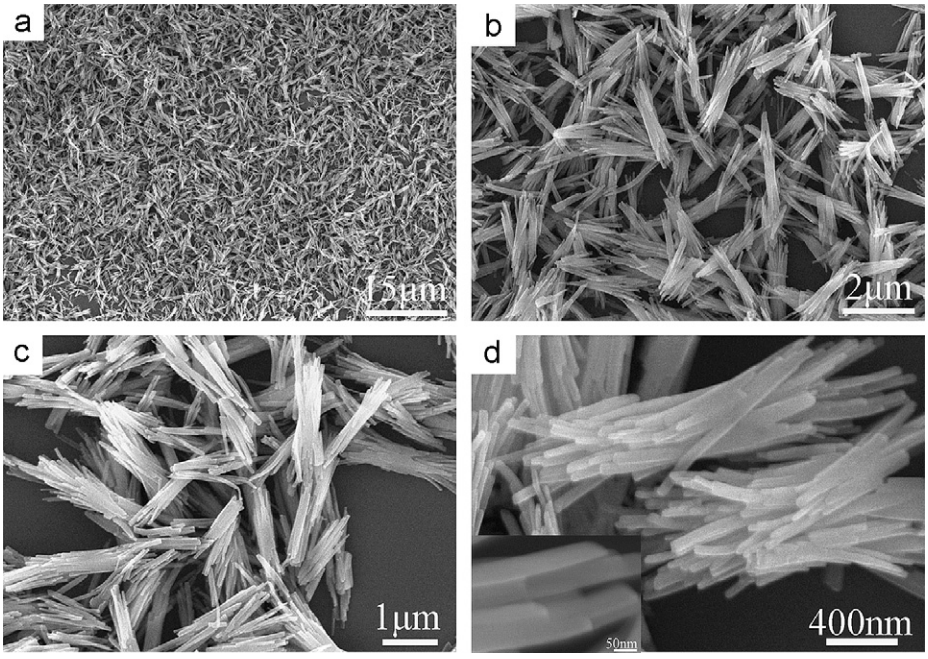

Fig. 7. SEM images of the La(1,3,5-BTC)$(H_2O)_6$ bundlelike architectures at different magnifications (ethanol, 40 mL).

flowerlike, wheatearlike, spherical, sheaflike, taillike, bundlelike architectures, and 1D nanorods of sizes and morphologies similar to the La(1,3,5-BTC)$(H_2O)_6$ were obtained (Fig. S4), indicating that activator ions (Eu^{3+}/Tb^{3+}) have little influence on the morphology of the La(1,3,5-BTC)$(H_2O)_6$ system.

3.3. *Tunable photoluminescence of the La(1,3,5-BTC)$(H_2O)_6$:Eu^{3+},Tb^{3+}*

When the Tb^{3+}/Eu^{3+} ions are doped into the La(1,3,5-BTC)$(H_2O)_6$ nano/micromaterials, the La(1,3,5-BTC)$(H_2O)_6$:5% Tb^{3+}(1%Eu^{3+}) emit green (red) light under UV excitation, which have been observed in our reported work [18]. The excitation spectrum consists of a broadband (200–330 nm) and some weak lines in the range from 330 to 500 nm (Fig. S5). The emission spectra of the La(1,3,5-BTC)$(H_2O)_6$:5%Tb^{3+}(1%Eu^{3+}) excited at 268 nm exhibits characteristic emissions of the Tb^{3+}/Eu^{3+} ions (Fig. 8). In addition, the characteristic emission from 1,3,5-BTC ligands disappears when the excitation wavelength is kept at 268 nm in the La(1,3,5-BTC)$(H_2O)_6$:5%Tb^{3+}(1%Eu^{3+}) samples, indicating the efficient energy transfer from the ligands to the Tb^{3+} (1%Eu^{3+}) ions.

In order to study the tunable photoluminescence properties of the system, we carried out co-doping Eu^{3+} and Tb^{3+} ions into the La(1,3,5-BTC)$(H_2O)_6$ host. Fig. 8 shows the emission spectra of La(1,3,5-BTC)$(H_2O)_6$:1%Eu^{3+}, x%Tb^{3+} ($x=1$–9%) under 268 nm

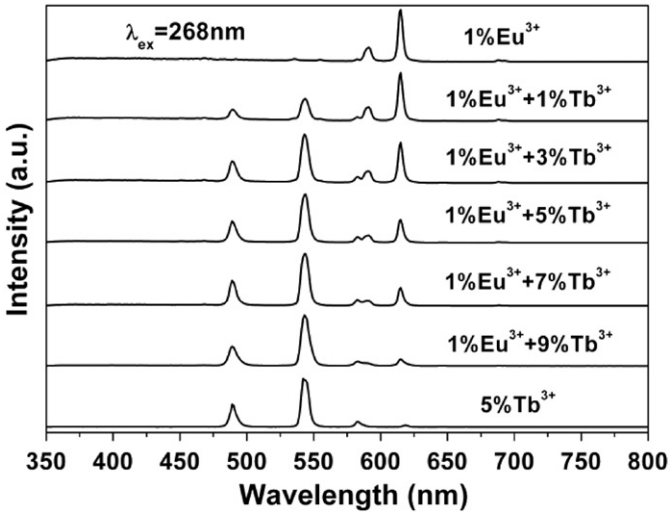

Fig. 8. PL emission spectra of the La(1,3,5-BTC)$(H_2O)_6$:Eu^{3+},Tb^{3+} solid samples.

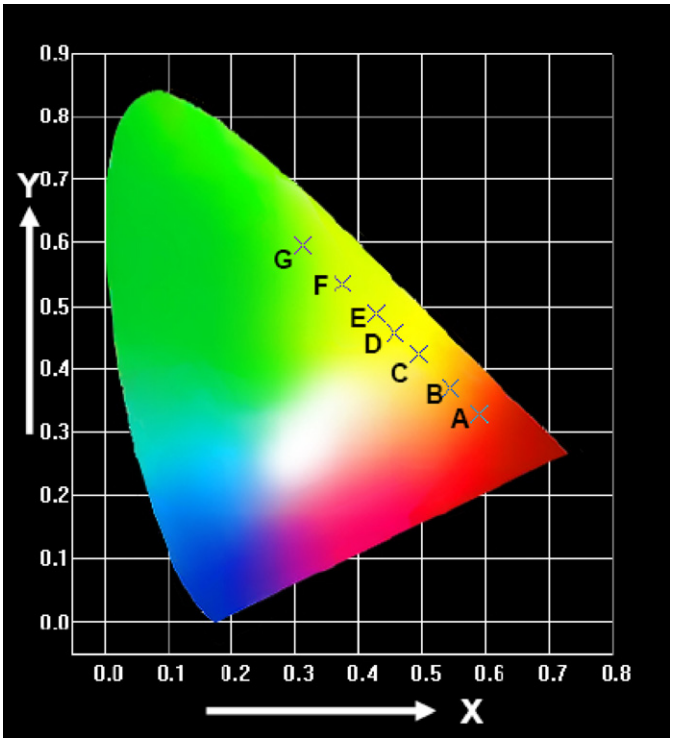

Fig. 9. CIE chromaticity diagram for the La(1,3,5-BTC)$(H_2O)_6$:1%Eu^{3+} (A), La(1,3,5-BTC)$(H_2O)_6$:1%Eu^{3+}, 1%Tb^{3+} (B), La(1,3,5-BTC)$(H_2O)_6$:1%Eu^{3+}, 3%Tb^{3+} (C), La(1,3,5-BTC)$(H_2O)_6$:1%Eu^{3+}, 5%Tb^{3+} (D), La(1,3,5-BTC)$(H_2O)_6$:1%Eu^{3+}, 7%Tb^{3+} (E), La(1,3,5-BTC)$(H_2O)_6$:1%Eu^{3+}, 9%Tb^{3+} (F), and La(1,3,5-BTC)$(H_2O)_6$:5%Tb^{3+} (G).

excitation. With the co-doping of the Tb^{3+} ions ($x=1$ mol%), besides the Eu^{3+} emissions, we can observe the characteristic emissions of the Tb^{3+} ions in these nano/microstructures. With the increase of the Tb^{3+} ions concentration, the luminescence of the Eu^{3+} ions begins to decrease, and that of the Tb^{3+} ions increases. When the doping concentration of the Tb^{3+} ions is 9%, the luminescence of the Eu^{3+} ions decreases obviously, while that of the Tb^{3+} ions keeps almost constant.

Therefore, the different photoluminescence colors can be realized from red, orange, yellow, green-yellow to green through simply adjusting the concentrations of the codoped Tb^{3+} and Eu^{3+} ions under the excitation wavelength of 268 nm in these superstructures by virtue of the efficient energy transfer from the La(1,3,5-BTC)$(H_2O)_6$ host lattice to the codoped Tb^{3+} and Eu^{3+}. Fig. 9 shows the corresponding CIE chromaticity diagram of La(1,3,5-BTC)$(H_2O)_6$:Eu^{3+},Tb^{3+} phosphors with different doping concentrations of the codoped activators. The corresponding luminescence colors can be seen clearly from the photographs of the La(1,3,5-BTC)$(H_2O)_6$:Eu^{3+},Tb^{3+} samples (Fig. S6) where a 254 nm UV lamp was used as an excitation source.

4. Conclusions

We have demonstrated a simple, mild one-step approach for the selective synthesis of novel 3D flowerlike, wheatearlike, spherical, sheaflike, taillike, bundlelike superstructures and 1D nanorods of the coordination polymer lanthanum 1,3,5-benzenetricarboxylate. The morphology evolution and fractal splitting level of La(1,3,5-BTC)$(H_2O)_6$ are strongly dependent on the reaction conditions such as concentration, molar ratio of reactants, surfactant, and solvent. The photoluminescence properties of isostructural La(1,3,5-BTC)$(H_2O)_6$:Eu^{3+},Tb^{3+} nano/microstructures were investigated in detail. More interestingly, the luminescent color can thus be easily modulated from red, orange, yellow, green-yellow to green due to different composition of emissions of Tb^{3+} and Eu^{3+}. Thus, our study may open a new and convenient pathway for tuning the luminescence properties in the visible region by selecting the appropriate metal–organic host materials and activator ions. Moreover, the advantage of the approach includes simplicity, high speed, high quality, ease of scale up, good reproducibility, and low cost. Thus, we believe that such methods may be extended to the synthesis of other nano/micro-scaled metal–organic materials with novel morphologies and fantastic properties.

Acknowledgments

This work is financially supported by the National Natural Science Foundation of China (Grant no. 20771098) and the Fund for Creative Research Groups (Grant no. 20921002), and the National Basic Research Program of China (973 Program, Grant no. 2007CB935502).

Appendix A. Supporting information

Supplementary data associated with this article can be found in the online version at doi:10.1016/j.jssc.2010.07.040.

References

[1] (a) O.M. Yaghi, M. Obkeeffe, N.W. Ockwig, H.K. Chae, M. Eddaoudi, J. Kim, Nature 423 (2003) 705;
(b) X. Zhao, B. Xiao, A.J. Fletcher, K.M. Thomas, D. Bradshaw, M.J. Rosseinsky, Science 306 (2004) 1012.
[2] (a) J.S. Seo, D. Whang, H. Lee, S.I. Jun, J. Oh, Y.J. Jeon, K. Kim, Nature 404 (2000) 982;
(b) M.D. Allendorf, C.A. Bauer, R.K. Bhaktaa, R.J.T. Houka, Chem. Soc. Rev. 38 (2009) 1330.
[3] (a) O.R. Evans, W. Lin, Acc. Chem. Res. 35 (2002) 511;
(b) J.P. Zou, G.W. Zhou, X. Zhang, M.S. Wang, Y.B. Lu, W.W. Zhou, Z.J. Zhang, G.C. Guo, J.S. Huang, CrystEngCommun 11 (2009) 972.
[4] (a) F.M. Tabellion, S.R. Seidel, A.M. Arif, P.J. Stang, J. Am. Chem. Soc. 123 (2001) 7740;
(b) M.E. Kosal, J.H. Chou, S.R. Wilson, K.S. Suslick, Nat. Mater. 1 (2002) 118.
[5] (a) M. Oh, C.A. Mirkin, Nature 438 (2005) 651;
(b) Y.M. Jeon, J. Heo, C.A. Mirkin, J. Am. Chem. Soc. 129 (2007) 7480.
[6] Z. Ni, R.I. Masel, J. Am. Chem. Soc. 128 (2006) 12394.

[7] (a) W.J. Rieter, K.M.L. Taylor, W.B. Lin, J. Am. Chem. Soc. 129 (2007) 9852;
(b) K.M.L. Taylor, A. Jin, W.B. Lin, Angew. Chem. Int. Ed. 47 (2008) 7722.
[8] (a) W. Cho, H.J. Lee, M. Oh, J. Am. Chem. Soc. 130 (2008) 16943;
(b) H.J. Lee, W. Cho, S. Jung, M. Oh, Adv. Mater. 21 (2009) 674.
[9] Y.H. Wang, B. Li, Y.H. Liu, L.M. Zhang, Q.H. Zuo, L.F. Shi, Z.M. Su, Chem. Commun. (2009) 5868.
[10] A.M. Spokoyny, D. Kim, A. Sumrein, C.A. Mirkin, Chem. Soc. Rev. 38 (2009) 1218.
[11] W. Lin, W.J. Rieter, K.M.L. Taylor, Angew. Chem. Int. Ed. 48 (2009) 650.
[12] (a) Z. Wang, V.C. Kravtsov, M.J. Zaworotko, Angew. Chem. Int. Ed. 44 (2005) 2877;
(b) N.L. Rosi, J. Kim, M. Eddaoudi, B.L. Chen, M. Keeffe, O.M. Yaghi, J. Am. Chem. Soc. 127 (2005) 1504;
(c) B.L. Chen, L.B. Wang, F. Zapata, G.D. Qian, E.B. Lobkovsky, J. Am. Chem. Soc. 130 (2008) 6718.
[13] (a) Y.Y. Liu, J.F. Ma, J. Yang, Z.M. Su, Inorg. Chem. 46 (2007) 3027;
(b) X.D. Guo, G.S. Zhu, Z.Y. Li, Y. Chen, X.T. Li, S.L. Qiu, Inorg. Chem. 45 (2006) 4065;
(c) X.D. Guo, G.S. Zhu, Z.Y. Li, F.X. Sun, Z.H. Yang, S.L. Qiu, Chem. Commun. (2006) 3172.
[14] Y.H. Wen, J.K. Cheng, Y.L. Feng, J. Zhang, Z.J. Li, Y.G. Yao, Chin. J. Struct. Chem. 24 (2005) 1440.
[15] (a) Z.F. Chen, R.G. Xiong, J. Zhang, X.T. Chen, Z.L. Xue, X.Z. You, Inorg. Chem. 40 (2001) 4075;
(b) J. Yang, Q. Yue, G.D. Li, J.J. Cao, G.H. Li, J.S. Chen, Inorg. Chem. 45 (2006) 2857.
[16] (a) K. Liu, H.P. You, G. Jia, Y.H. Zheng, Y.H. Song, M. Yang, Y.J. Huang, H.J. Zhang, Cryst. Growth Des. 9 (2009) 3519;
(b) K. Liu, G. Jia, Y. Zheng, Y. Song, M. Yang, Y. Huang, L. Zhang, H. You, Inorg. Chem. Commun. 12 (2009) 1246;
(c) K. Liu, H.P. You, Y.H. Zheng, G. Jia, L.H. Zhang, Y.J. Huang, M. Yang, Y.H. Song, H.J. Zhang, Cryst. Eng. Commun. 11 (2009) 2622.
[17] (a) K. Liu, H.P. You, G. Jia, Y.H. Zheng, Y.J. Huang, Y.H. Song, M. Yang, L.H. Zhang, H.J. Zhang, Cryst. Growth Des. 10 (2010) 790;
(b) K. Liu, H.P. You, Y.H. Zheng, G. Jia, Y.H. Song, Y.J. Huang, M. Yang, J.J. Jia, N. Guo, H.J. Zhang, J. Mater. Chem. 20 (2010) 3272.
[18] K. Liu, H.P. You, Y.H. Zheng, G. Jia, Y.J. Huang, M. Yang, Y.H. Song, L.H. Zhang, H.J. Zhang, Cryst. Growth Des. 10 (2010) 16.
[19] J. Tang, A.P. Alivisatos, Nano Lett. 6 (2006) 2701.
[20] Y.O. Punin, Crystal splitting, Zap. Vses. Mineral. Ova. Part 110 (6), 666.
[21] Y.H. Kim, Y.W. Jun, B.H. Jun, S.M. Lee, J. Cheon, J. Am. Chem. Soc. 124 (2002) 13656.
[22] (a) X.F. Shen, X.P. Yan, Angew. Chem. Int. Ed. 46 (2007) 7659;
(b) H. Xue, Z.H. Li, H. Dong, L. Wu, X.X. Wang, X.Z. Fu, Cryst. Growth Des. 8 (2008) 4469.
[23] Z.P. Liu, S. Li, Y. Yang, S. Peng, Z.K. Hu, Y.T. Qian, Adv. Mater. 15 (2003) 1946.